



A Null-Filled Axisymmetric Secant-Square-Shaped Beam Antenna for Unmanned Aerial Vehicles

Weihao Diao , Yue Li , Senior Member, IEEE, and Zhijun Zhang , Fellow, IEEE

Abstract—In this letter, an antenna with a null-filled axisymmetric secant-square-shaped beam for the unmanned aerial vehicle is proposed. The proposed antenna consists of four monopoles with sequentially rotated feed and a coupling-fed grooved circular patch. The radiation power ratio of the monopoles and the patch is used to shape the axisymmetric beam. The effect of the ground is also investigated to operate positively on beam shaping. A prototype was fabricated to validate the method and the performance of the proposed antenna. The gain curves of the proposed antenna coincide well with the secant-squared (\sec^2) curve from $\theta = 0^\circ$ to $\theta = 60^\circ$ in all azimuthal angles with root mean square error (RMSE) below 1.35 dB in 5.5–5.7 GHz.

Index Terms—Axisymmetric beam, null-filled radiation pattern, secant-squared beam shaping, unmanned aerial vehicle (UAV).

I. INTRODUCTION

UNMANNED aerial vehicles (UAVs) gain popularity on account of their wide coverage, convenient deployment, and risky-task compatibility. Efficient communication between a UAV and the ground should be guaranteed.

A shaped beam is preferred for a UAV antenna. The schematic diagram of the scene mentioned above is illustrated in Fig. 1. The distance R , height H , and elevation angle θ satisfy the relationship: $R = H \sec \theta$. Therefore, the gain of the UAV antenna should be proportional to the square of $\sec \theta$ to compensate for the path loss. This is the so-called secant-squared beam shaping [1], [2], [3].

Owing to the flexible relative position between a UAV and a ground device, the radiation pattern of a UAV antenna should be axisymmetric. A monopole or a dipole as well as their variants can provide axisymmetric radiation [4], [5], [6], [7], [8]. However, their intrinsic broadside null should be filled to communicate with a ground device right below a UAV. The problem can be solved by pattern reconfigurable antennas [9], [10], [11], quadrifilar antennas [12], [13], or combining axisymmetric beam antennas with broadside antennas [14], [15], [16], [17], [18].

A reconfigurable antenna can switch its beam to cover a wide scope, whereas the feeding network may be complicated due to the switches and dc bias circuits. A quadrifilar antenna can readily be designed to shape its pattern and cover the upper

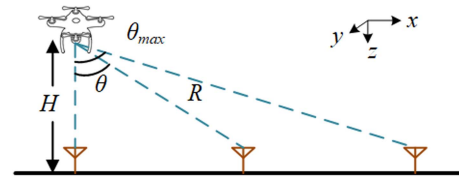


Fig. 1. Schematic diagram of the scene where a UAV communicates with devices on the ground.

hemisphere. Nevertheless, circularly polarized (CP) quadrifilar antennas match poorly with linearly polarized (LP) antennas that are usually applied on UAVs and the ground systems. There will be an additional 3 dB polarization-mismatch loss if a quadrifilar antenna is employed, which is undesired. When combining an axisymmetric antenna with a broadside antenna, the feeding network can be simple, and the polarization can be linear. So this method may be a good choice. The authors in [14], [15], [16], [17], and [18] utilized LP or CP broadside beams to fill the null of axisymmetric patterns with invariant radiation phases on latitude lines. This will cause the asymmetry of the radiation pattern. It would be better if the radiation phase of the two kinds of beams is aligned.

In this letter, an antenna with a null-filled axisymmetric secant-square-shaped pattern for UAVs is proposed. A conical beam and a CP broadside radiation pattern are, respectively, obtained by four monopoles with SRF and a grooved circular patch. The radiation phases of the monopoles and the patch on latitude lines are aligned, which are both rotationally varied. Thus, the axisymmetry of the radiation pattern will not degrade after combing the monopoles with SRF and the patch. A prototype was fabricated and measured. The root mean square error (RMSE) and maximum error (ME) of the gain curves to the \sec^2 curve are low in the desired band, pointing to a decent fitting.

II. ANTENNA DESIGN

The geometry of the proposed antenna is demonstrated in Fig. 2. The antenna is composed of four monopoles with SRF, a grooved circular metal patch, and a circular ground. The monopoles are fed by the microstrip feeding network shown in Fig. 2(d), and the patch is suspended to be coupling fed by the monopoles. The microstrip feeding network comprises three Wilkinson power dividers and some delay lines printed on the F4B substrate ($\epsilon_r = 2.65$, and $\tan \delta = 0.0015$). The detailed dimensions of the proposed antenna are listed in Table I.

First, the superposition of a vertical polarized (VP) axisymmetric beam and a CP broadside beam is investigated. The sources of the beams are on an infinite ground for a simple demonstration. The monopoles with SRF can provide a conical

Manuscript received 24 March 2023; accepted 19 April 2023. Date of publication 25 April 2023; date of current version 4 August 2023. This work was supported in part by the National Natural Science Foundation of China under Grant 61971254 and Grant 62271279. (Corresponding author: Zhijun Zhang.)

The authors are with the Department of Electronic Engineering, Tsinghua University, Beijing 100084, China, and also with the Beijing National Research Center for Information Science and Technology, Tsinghua University, Beijing 100084, China (e-mail: dwh21@mails.tsinghua.edu.cn; lyee@tsinghua.edu.cn; zjzh@tsinghua.edu.cn).

Digital Object Identifier 10.1109/LAWP.2023.3270028

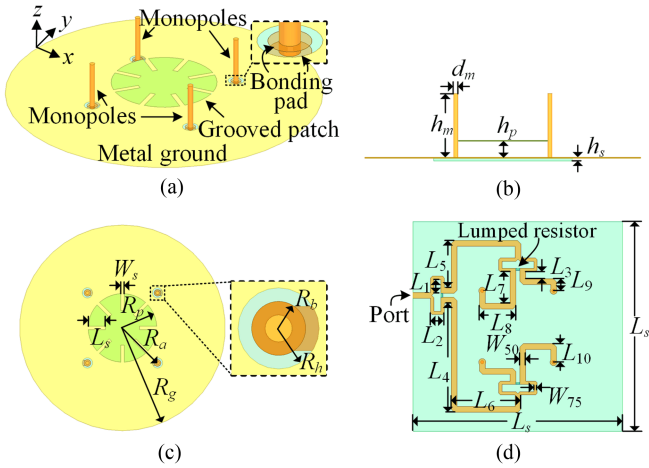


Fig. 2. Geometry of the proposed antenna. (a) Perspective view. (b) Front view. (c) Top view. (d) Feeding network.

TABLE I
DETAILED DIMENSIONS OF THE PROPOSED ANTENNA

Parameter	d_m	h_m	R_g	R_p	R_d	h_p
Value (mm)	1	10.9	122.5	10	14.5	2.8
Parameter	l_s	w_s	L_s	h_s	L_1	L_2
Value (mm)	5	1	60	0.6	4	3.9
Parameter	L_3	L_4	L_5	L_6	L_7	L_8
Value (mm)	2	31.3	13.5	19.9	9.1	10.5
Parameter	L_9	L_{10}	W_{50}	W_{75}	R_b	R_h
Value (mm)	3.4	5.3	1.64	0.92	1	1.5

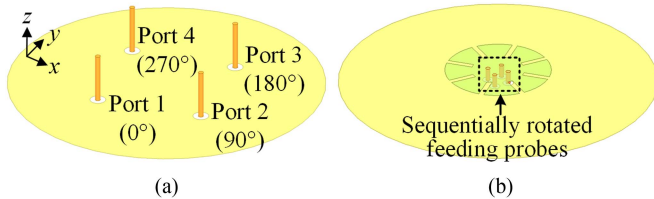


Fig. 3. (a) Monopoles with SRF. (b) CP patch.

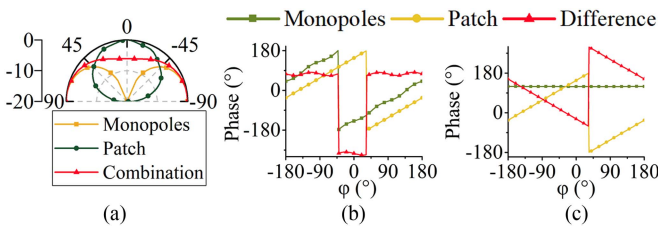


Fig. 4. (a) Radiation pattern in xoz -plane of the monopoles, the patch, and the combination of the two. (b) Radiation phases in the SRF case and (c) in-phase feed case.

pattern as illustrated in Figs. 3(a) and 4(a). On the infinite sphere, the radiation phase distribution of the monopoles on any latitude line (where coordinate θ is constant and φ varies only) is rotationally varied. It can be seen in Fig. 4(b) (the green line) that the radiation phase will change by one period when azimuthal coordinate φ turns one round. As a comparison, the radiation phase of four identical monopoles fed in phase is plotted in Fig. 4(c) (the green line), which is constant on any latitude line.

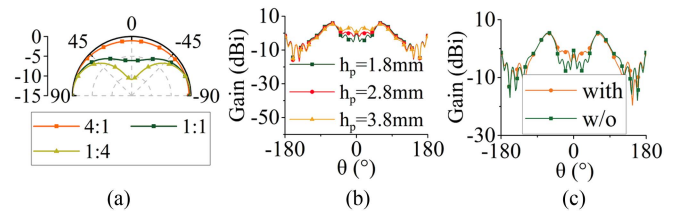


Fig. 5. Radiation patterns of in xoz -plane (a) with different power ratios in the ideal case, (b) of the proposed antenna with different patch height, and (c) of the propose antenna with and without the patch.

The grooved circular patch can provide a CP broadside beam to fill the null of the monopoles, as shown in Figs. 3(b) and 4(a). In Fig. 3(b), SRF is used to excite the CP mode to facilitate the demonstration. Note that the feeding probes shown in Fig. 3(b) only serves to obtain a CP broadside beam with a single patch in simulation, and the final feeding scheme of the patch is coupling feed because the field in the area surrounded by the monopoles can excite the CP mode of the patch. As shown in Fig. 4(b) and (c) (the yellow lines), the phase of the E_θ component is rotationally varied like that of monopoles with SRF. The phase of the E_φ component is also rotationally varied, which is omitted in Fig. 4 for clarity. The radiation phase differences between the monopoles and the patch are plotted in Fig. 4(b) and (c) (the red lines). As shown, the phase difference in the SRF case is almost constant, while that in the in-phase-feed case varies by one period. Thus, the radiation field of the monopoles with SRF and the patch will never be canceled out in any direction if the phase difference is proper. In contrast, the radiation field of the in-phase fed monopoles and the patch will always be canceled out in a certain direction, leading to a dip in the pattern. This is the flaw in [13], [14], and [15]. As for [11] and [12], LP beams are used to fill the null. The patterns in [11] and [12] are asymmetric because linear polarization is not rotationally symmetric.

Next, the method to shape the beam is presented, which is adjusting the power ratio between the patch and the monopoles. Fig. 5(a) illustrates the patterns generated by the combination of the antennas in Fig. 3(a) and (b) with different power ratios. The more power radiated by the patch, the higher the broadside gain is. For coupling feed, the power ratio can be tuned by the height of the patch with little effect on other performances, as shown in Fig. 5(b). The near E-field of a monopole is mainly parallel to the ground, which will be suppressed at the vicinity of the ground. Hence, a lower patch means a weaker coupling. The size of the patch can also be used, but the operating frequency will be affected. Fig. 5(c) depicts the actual radiation pattern in xoz -plane of the proposed antenna with and without the patch. With the patch, the gain near the broadside is improved and the ripple is lower than that of the antenna without the patch. It should be noted that the patch is grooved for miniaturization to obtain a wider beam and a proper power ratio. As shown in the inset of Fig. 6(b), the radial slots can elongate the current path, thus lowering the resonant frequency of the patch. The active reflection coefficients shown in Fig. 6(a) are attained by the model in Fig. 3(b) with and without slots. The working band is lower than the resonant frequency of the patch because, in sec^2 beam shaping, the broadside gain should not be high. But the resonant frequency of the patch without slots is too high, leading to weak coupling. By etching radial slots, the resonant

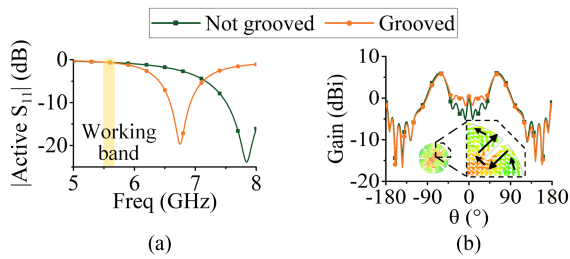


Fig. 6. (a) Resonant frequencies of the patch with and without slots. (b) Radiation patterns in xoz -plane of the proposed antenna with the grooved patch and the patch not grooved.

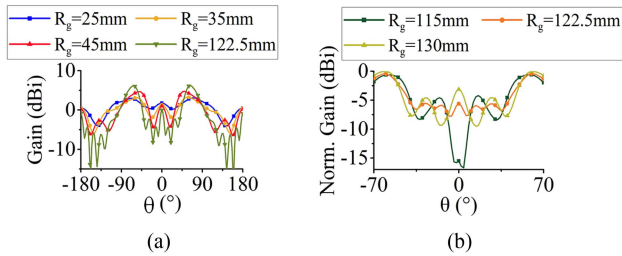


Fig. 7. Radiation patterns in xoz -plane of the proposed antenna (a) without the patch in different ground sizes, and (c) with the patch in different ground sizes.

frequency of the patch can be lowered for a proper power ratio and the beamwidth will not be narrowed for low ripple. It should be noted that in Fig. 6(b), the gain rises abruptly on the broadside. On account of the SRF, the diffraction field on the ground edge will be constructively superimposed in broadside to radiate a circular polarization field like that of a circular patch. The radiation patterns of the proposed antenna without the patch in different ground sizes are depicted in Fig. 7(a). It can be observed that a smaller ground leads to a higher gain near the broadside. Thus, the null can be filled by a small ground. However, the reduction of the ground will make the maximum gain decrease, and more energy radiated in the unwanted direction. Moreover, the beam shaping is carried out within the coverage (from the broadside to the maximum gain direction). When the size of the ground decreases, the maximum gain direction will get close to the broadside, indicating coverage shrinkage. The degradation caused by the small ground for null filling contradicts with application consideration. Hence, filling the null with only a small ground is not applicable although simpler. The radiation patterns of the proposed antenna with the patch in different sizes of ground are plotted in Fig. 7(b). As shown, the gain near the broadside varies drastically with the size of the ground, while the gain in other directions varies slightly. This is because the broadside gain will be high with the edge field of the ground and the patch being in-phase, while that will be low in the out-of-phase case. When the size of the ground is determined, the shape of the radiation pattern can always be adapted appropriately by the patch.

III. SIMULATED AND MEASURED RESULTS

A prototype of the proposed antenna was fabricated as shown in Fig. 8. The grooved patch is supported by foam ($\epsilon_r \approx 1$). The microstrip feeding network is located in the center hollow of the circular metal plate and they are cogrounded by brass tapes in the bottom. A 50Ω coaxial cable is used for energy input.

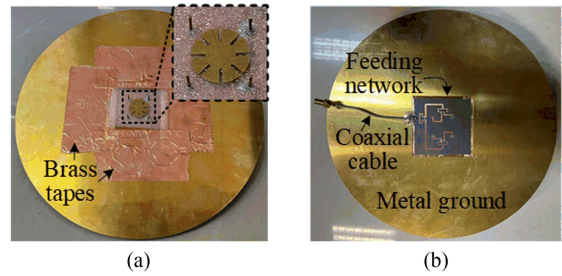


Fig. 8. Photograph of the proposed antenna. (a) Perspective view. (b) Back view.

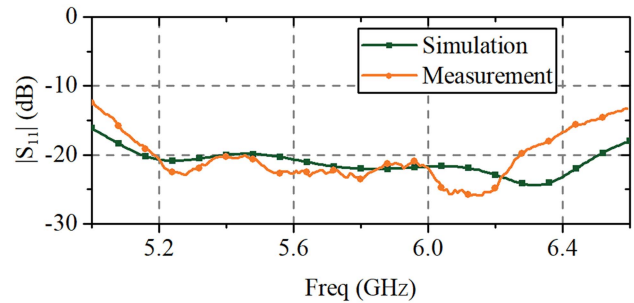


Fig. 9. Reflection coefficient of the proposed antenna.

The simulated and measured reflection coefficients of the proposed antenna are shown in Fig. 9. It can be seen that the proposed antenna is well matched in the band of interest. Fig. 10 depicts the simulated and measured radiation patterns of the proposed antenna in xoz -plane at different frequencies. The broadside gain is higher with a higher frequency due to a stronger coupling. Additionally, the direction of the maximum gain occurs at $\theta = 60^\circ$.

To evaluate the fitting of the patterns to the \sec^2 curve in all elevation planes, the gain curves in 36 different sampling elevation planes ($\varphi = 0^\circ, 10^\circ, 20^\circ, \dots, 350^\circ$) are plotted in Fig. 9. At a single frequency, 36 curves of gain are plotted in the same figure to fit the \sec^2 curve. Because the maximum gain occurs at $\theta = 60^\circ$, the range from $\theta = 0^\circ$ to $\theta = 60^\circ$ is where the performance of beam shaping is investigated. The expression of a \sec^2 curve is as follows:

$$G_{\sec^2} = C + 20 \lg(\sec \theta), 0^\circ \leq \theta \leq 60^\circ. \quad (1)$$

The final C is chosen to be the average of that obtained with least square method in 5.5, 5.6, and 5.7 GHz, which is -1.4 dB. The fitness of the gain curves in all 36 elevation planes to the \sec^2 curve is evaluated by the RMSE. As shown in Fig. 11, the gain curves in 5.5–5.7 GHz all fit the \sec^2 curve well. The RMSEs at 5.5, 5.6, and 5.7 GHz, respectively, are 1.35, 0.76, and 1.14 dB in simulation and 1.23, 0.89, and 1.20 dB in measurement. The axisymmetry of the radiation pattern from $\theta = 0^\circ$ to $\theta = 60^\circ$ can be reflected by the dispersion of the cluster of the gain curves. Therefore, the RMSE can quantify the performance of beam-shaping and axisymmetry. A lower RMSE means better fitness and axisymmetry. The RMSEs, gains, and efficiencies at different frequencies are depicted in Fig. 10. The RMSE becomes higher when the frequency deviates from the center frequency 5.6 GHz. The reason is that the exciting amplitudes

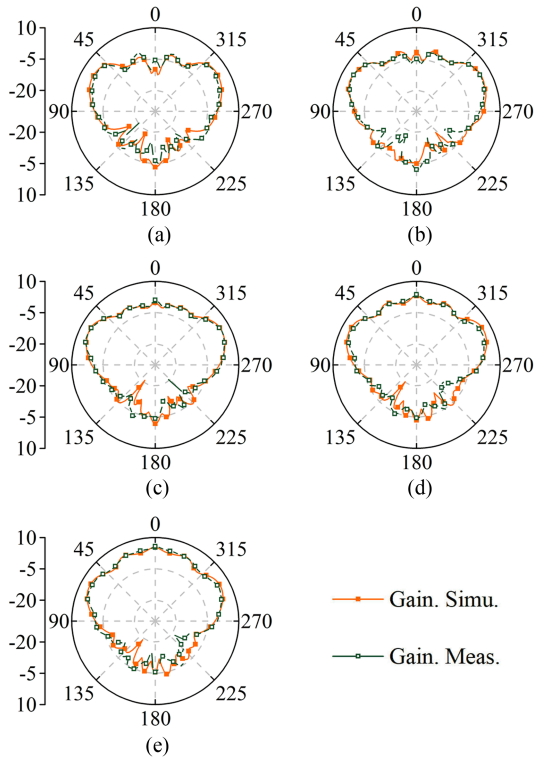


Fig. 10. Simulated and measured patterns of the proposed antenna in xoz -plane at (a) 5.4. (b) 5.5. (c) 5.6. (d) 5.7, and (e) 5.8 GHz.

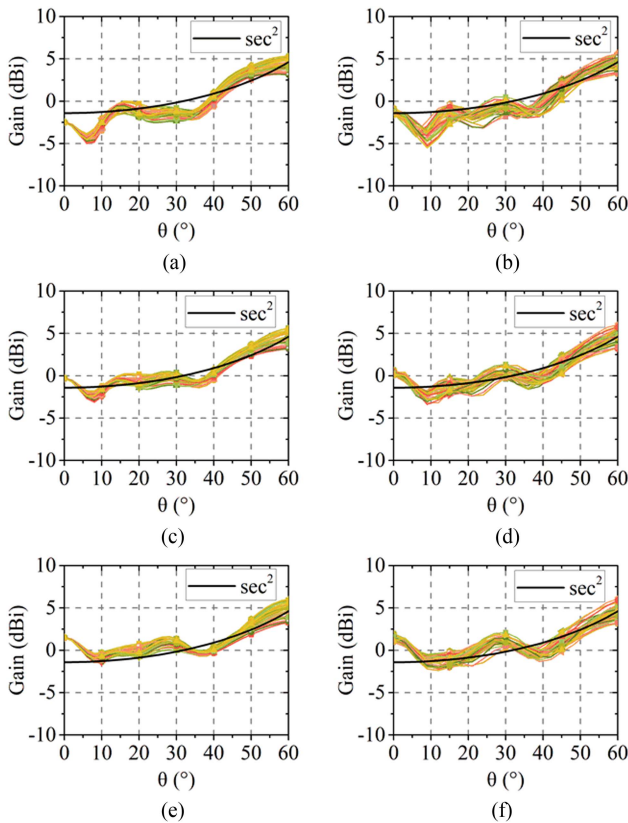


Fig. 11. Simulated and measured gain curves of the proposed antenna in 36 elevation planes. (a) Simulated 5.5 GHz. (b) Measured 5.5 GHz. (c) Simulated 5.6 GHz. (d) Measured 5.6 GHz. (e) Simulated 5.7 GHz. (f) Measured 5.7 GHz.

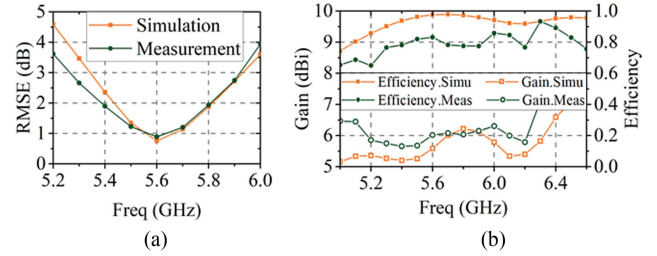


Fig. 12. (a) Simulated and measured RMSE of the proposed antenna. (b) Simulation and measurement gain and efficiencies of the proposed antenna.

TABLE II
COMPARISON AMONG THE PROPOSED WORK AND OTHER WORKS

Reference	Null-filling Method	RMSE (dB)	ME (dB)
[11]	Monopole + coupled rings	3.15	6.67
[12]	Bowtie slots + circular slot	3.46	8.98
[13]	VP cavities + annular strip	2.97	5.37
[14]	Monocone + spiral slot	4.91	13.32
[15]	CP cavity + annular strip	2.00	3.80
This work	Rotational fed monopoles + CP patch	0.89	2.91

and phases of the four ports will change with the frequency. All the measured results agree well with the simulated results. The slight differences between them may be caused by fabrication tolerances.

Table II compares the performances of this work and other works. The MEs at the corresponding center frequencies are calculated to evaluate the performances of beam-shaping for a thorough perspective of view. In the references, the RMSEs and the MEs are not given, so they are manually calculated by the authors from the data of the references. It should be noted that radiation patterns in only one or two elevation planes are given in the references, so the RMSEs and MEs in Table II are that of the given 2-D patterns. And actual RMSEs and MEs may be higher. It can be seen that not only the RMSE but also the ME of the radiation pattern are the lowest. Generally, the radiation patterns of the proposed antenna fit the \sec^2 curve nicely in all azimuthal angles.

IV. CONCLUSION

In this letter, a null-filled axisymmetric secant-squared beam-shaped antenna is proposed. Four monopoles with SRF can provide the radiation phase distributions varying in step with that of the grooved circular patch, leading to good axisymmetry. The height of the patch is used to shape the beam to fit the \sec^2 curve. The measured results show that the proposed antenna can radiate an axisymmetric \sec^2 -shaped beam in a wide range. Both the RMSE and the ME of the gain curves are remarkably low, indicating an extraordinary fitting in all azimuthal angles.

REFERENCES

- [1] C. C. Cruz, C. A. Fernandes, S. A. Matos, and J. R. Costa, "Synthesis of shaped-beam radiation patterns at millimeter-waves using transmit arrays," *IEEE Trans. Antennas Propag.*, vol. 66, no. 8, pp. 4017–4024, Aug. 2018.
- [2] R. Sauleau and B. Bares, "A complete procedure for the design and optimization of arbitrarily shaped integrated lens antennas," *IEEE Trans. Antennas Propag.*, vol. 54, no. 4, pp. 1122–1133, Apr. 2006.

- [3] Y. Ren, X. Luan, Z. Wang, and K. Tan, "Research on the secant squared beamforming antenna for building coverage," in *Proc. Int. Conf. Microw. Millimeter Wave Technol.*, 2019, pp. 1–3.
- [4] H.-T. Chou, D.-B. Lin, and H.-L. Chiu, "Planar dual-mode dipole antenna formed by artificial microstrip arms loaded with multiple H-slots for broadband operation of vertically polarized radiation on UAV platform," *IEEE Trans. Antennas Propag.*, vol. 70, no. 9, pp. 7869–7877, Sep. 2022.
- [5] M. Nosrati, A. Jafargholi, R. Pazoki, and N. Tavassolian, "Broadband slotted blade dipole antenna for airborne UAV applications," *IEEE Trans. Antennas Propag.*, vol. 66, no. 8, pp. 3857–3864, Aug. 2018.
- [6] L. Sun, B. Sun, J. Yuan, W. Tang, and H. Wu, "Low-profile, quasi-omnidirectional substrate integrated waveguide (SIW) multihorn antenna," *IEEE Antennas Wireless Propag. Lett.*, vol. 15, pp. 818–821, 2016.
- [7] P. Liu, Z. Meng, L. Wang, Y. Zhang, and Y. Li, "Omnidirectional dual-polarized saber antenna with low wind drag," *IEEE Trans. Antennas Propag.*, vol. 68, no. 1, pp. 558–563, Jan. 2020.
- [8] Y. Zhang, P. Liu, Y. Yin, and Y. Li, "Omnidirectional dual-polarized antenna using colocated slots with wedgy profile," *IEEE Trans. Antennas Propag.*, vol. 69, no. 9, pp. 5446–5454, Sep. 2021.
- [9] W. Zhang, Y. Li, Z. Zhang, and Z. Feng, "A pattern-reconfigurable aircraft antenna with low wind drag," *IEEE Trans. Antennas Propag.*, vol. 68, no. 6, pp. 4397–4405, Jun. 2020.
- [10] W. Lin, H. Wong, and R. W. Ziolkowski, "Wideband pattern-reconfigurable antenna with switchable broadside and conical beams," *IEEE Antennas Wireless Propag. Lett.*, vol. 16, pp. 2638–2641, 2017.
- [11] Y. Ji, L. Ge, Y. Li, and J. Wang, "Wideband polarization agile dielectric resonator antenna with reconfigurable broadside and conical beams," *IEEE Trans. Antennas Propag.*, vol. 70, no. 8, pp. 7169–7174, Aug. 2022.
- [12] A. M. Musthafa, M. Khalily, A. Araghi, O. Yurduseven, and R. Tafazolli, "Compact multimode quadrifilar helical antenna for GNSS-R applications," *IEEE Antennas Wireless Propag. Lett.*, vol. 21, no. 4, pp. 755–759, Apr. 2022.
- [13] Y. Tawk, M. Chahoud, M. Fadous, J. Costantine, and C. G. Christodoulou, "The miniaturization of a partially 3-D printed quadrifilar helix antenna," *IEEE Trans. Antennas Propag.*, vol. 65, no. 10, pp. 5043–5051, Oct. 2017.
- [14] J. H. Bang, "Wideband low-profile null-filled monopole antenna for aircraft flush-mount applications," *Electron. Lett.*, vol. 51, no. 21, pp. 1635–1637, Oct. 2015.
- [15] M. Sadiq, S. Ullah, and C.-J. Ruan, "Null-filled shaped beam horizontally polarized omnidirectional antenna," in *Proc. Photon. Electromagn. Res. Symp.*, 2019, pp. 464–469.
- [16] H. Nawaz, X. Liang, M. S. Sadiq, J. Geng, W. Zhu, and R. Jin, "Ruggedized planar monopole antenna with a null-filled shaped beam," *IEEE Antennas Wireless Propag. Lett.*, vol. 17, no. 5, pp. 933–936, May 2018.
- [17] W. Kim, G. Shin, K.-W. Lee, B. Mun, and I.-J. Yoon, "A wideband monoconical antenna for airborne applications with a null-filled radiation pattern," *IEEE Antennas Wireless Propag. Lett.*, vol. 21, no. 6, pp. 1158–1162, Jun. 2022.
- [18] H. Nawaz, X. Liang, M. S. Sadiq, J. Geng, and R. Jin, "Circularly-polarized shaped pattern planar antenna for aerial platforms," *IEEE Access*, vol. 8, pp. 7466–7472, 2020.
- [19] Y. Zhang and Y. Li, "Wideband isotropic antenna with miniaturized ground for enhanced 3-dB coverage ratio," *IEEE Antennas Wireless Propag. Lett.*, vol. 21, no. 6, pp. 1253–1257, Jun. 2022.
- [20] J. Yu, W.-J. Lu, Y. Cheng, and L. Zhu, "Dual-resonant wideband microstrip annular sector patch antenna with increased backfire radiations," *IEEE Trans. Antennas Propag.*, vol. 70, no. 6, pp. 4181–4188, Jun. 2022.
- [21] Y. Li, Z. Zhang, and Z. Feng, "A sequential-phase feed using a circularly polarized shorted loop structure," *IEEE Trans. Antennas Propag.*, vol. 61, no. 3, pp. 1443–1447, Mar. 2013.
- [22] J. L. Volakis, *Antenna Engineering Handbook*, 4th ed. New York, NY, USA: McGraw-Hill, 2007, pp. 10–11.